Two-dimensional magnetoexcitons in type-II semiconductor quantum dots

Marcos H. Degani,[1,*] Marcelo Z. Maialle,[2] Gilberto Medeiros-Ribeiro,[3] and Evaldo Ribeiro[4]
[1]*Haras Degani, Av. Fioravante Piovani 1000, Itatiba-SP, 13257-700, Brazil*
[2]*Liceu Vivere, R. Duque de Caxias Norte 550, Pirassununga-SP, 13635-000, Brazil*
[3]*Laboratório Nacional de Luz Síncrotron, C.P. 6192, Campinas-SP, 13084-971, Brazil*
[4]*Departamento de Física, Universidade Federal do Paraná, C.P. 19044, Curitiba-PR, 81531-990, Brazil*
(Received 7 March 2008; revised manuscript received 16 May 2008; published 25 August 2008)

We have investigated the excitons formed in planar type-II semiconductor structures as function of an applied magnetic field. The type-II structure studied confines the electron inside a quantum dot and keeps the hole outside; the exciton is formed by the electron-hole Coulomb attraction. The shape of the dots is varied from circular to ellipsoidal, with smooth or rough potential walls. The effects of a lattice defect and of a shallow hydrogenic impurity located close the dot are also investigated. The problem is solved numerically for two interacting particles in a two-dimensional model with the magnetic field aligned perpendicularly to the dot plane. A simpler solution with separable wave functions for the electron and the hole was used to obtain the contributions of the excited states. The exciton spectra exhibit many energy-level crossings with angular-momentum changes in agreement with the Aharonov-Bohm effect. Our results for systems with reduced symmetry (elliptical and/or rough quantum dots or with the impurity or defect) have shown anticrossings of the exciton energy levels, leading to modulations on the average energy and on the optical oscillator strength of the exciton as function of the magnetic field. Similar modulations have been observed for type-II quantum dots and they were discussed considering the reduced dot symmetry and a selective optical excitation and relaxation processes contributing to the photoluminescence signal.

DOI: 10.1103/PhysRevB.78.075322 PACS number(s): 71.35.Ji, 78.67.Hc, 73.22.Dj

I. INTRODUCTION

Quantum dots (QDs) can be grown in semiconductors by different techniques and they have attracted a great deal of attention from academical and technological viewpoints. The interest, in both cases, resides mostly on the possibility of controlling the physical dimensions of the system, which ultimately dictate the quantum level structure of the dots. Common results from planar growth techniques are QDs of cylindrical, semispherical, or pyramidallike shapes, for which the dot bases are much larger than the heights, that is, the dots are predominantly flat.

If the choice of materials is such that the band offset potential confines one charged carrier—say the electron in the conduction band—inside the dot region and the opposite-charged carrier—now the hole in the valence band—stays outside this region, one has the so-called type-II QD. In this case, the hole stays close to the electron due to the Coulomb attraction and they form an exciton having a long lifetime because of the small oscillator strength for optical transition, which demands overlap between the electron and hole wave functions. Spatially indirect excitons with their long lifetimes are desirable for many applications, such as in memory devices for optical computing, therefore justifying the interest in type-II QDs.

There have been some studies of excitons in type-II QDs under applied magnetic field motivated also by the charge spatial separation, which would allow the observation of the exciton Aharonov-Bohm effect (X-ABE),[1,2] i.e., an oscillatory behavior of the exciton ground state for varying B,[3] with the oscillation period related to the magnetic-flux quantum h/e passing through an excluded region inside the ringlike wave functions of the carriers. There is still a debate if the exciton state in type-II QD has the outside charged carrier distributed laterally around the QD or on the top/bottom of the QD. These different configurations can lead to different behaviors when a magnetic field is applied along the growth direction, favoring or not the observation of the X-ABE.

In real type-II QD systems the understanding of the carrier distribution around and inside the QD is complicated by the role of some aspects of the growth process, affecting mostly the strain-induced potentials and the geometry of the QDs. As a way of ensuring the outside carrier stays around the QD, there are proposals of creating potential barriers close to the top/bottom of the QD (Refs. 4 and 5) and a proposal with stacked quantum dots.[6] In these cases, and others in which the strain may act in the same way favoring a planar carrier distribution,[7] a simple picture for the exciton can be that in which one carrier is found inside a flat disk with an opposite-charged carrier around it in a ringlike distribution. If that is the case, the system should be quite well described by a two-dimensional model.

Interestingly, experimental studies of type-II QDs have shown data from optical measurements with modulations produced by the magnetic field,[6,8] appearing both on the average exciton energy, as well as on the intensity of the photoluminescence (PL), the latter in a stronger degree. Another study[9] has not reported such modulations maybe because the exciton charge distribution, as discussed above, did not favor them. The observed modulations have been linked to the changes on the angular momentum undergone by the ground-state exciton as in the X-ABE. However, it is still not clear how the modulations should appear in optical measurements. The existing theoretical models,[10] although yielding energy-level crossings associated to different angular-momentum components, have not predicted B-field modulations on the PL spectra for circular-shaped dots. Calculations for circular

type-II quantum rings,[11] including the finite-size width of them, have predicted *B*-field modulations for the optically bright exciton energy originated by the changes in the spatial confinement of the hole (outside carrier), which can go from the inside to the outside of the regions delimited by the ring. The results were discussed in terms of the second derivative and of the persistent current; the PL spectra were not discussed.

Restrictions on the cylindrical symmetry of the QD allow interactions between the energy levels of different angular momenta, producing level anticrossings, and they seem to be the origin of the *B*-field modulations in the PL measurements. Indeed, the existing calculation done for an impurity-induced symmetry breaking,[12] using a simplified model of the type-II QD, predicted a small effect on the PL intensity. However, even the prediction of this small effect is actually surprising because, as it is discussed in this paper, the way the PL intensity was calculated favors the partial fulfillment of a sum rule for the optical oscillator strength, which tends to hide the *B*-field modulations on the PL signal, as we will discuss below.

In the present work, we investigated an exciton in a type-II circularlike QD with the electron inside the dot and the hole around it. We used a two-dimensional model to investigate the effects of the applied magnetic field on the exciton. The Coulomb interaction is treated using separable wave functions for the electron and hole, after we have checked that an exact calculation with two interacting particles reproduced our results with the separable wave functions. We have calculated the overlap between the electron and hole wave functions to obtain the optical oscillator strength of the exciton. It is observed that only the hole states of cylindrical symmetry (orbital angular momentum $L_z=0$) contributed appreciably to the optical recombination process. Neglecting possible effects of crystal asymmetry and/or strain, we did not observe any *B*-field modulations in the PL spectra for perfectly circular QDs, for which the energy spectra showed actual crossings of the energy levels of different angular momenta. When the cylindrical symmetry is broken, which in our case is done by considering elliptical QDs, rough potential walls, impurities, and defect potentials, the energy levels with different angular-momentum components interact, producing anticrossings of levels which may be the origin of the observed *B*-field modulations in the PL spectra. This, however, demands a situation in which a partial sum rule existing in the PL intensity calculation cannot be fulfilled. We put forward a tentative interpretation of the observed *B*-field modulations considering a selective process for the optical excitation and the subsequent relaxation dynamics leading to the PL signal.

This paper is organized as follows. In the next section (Sec. II) we described the type-II QD system and the method used to obtain the exciton states. In Sec. III the results for the energy levels and the optical oscillator strength of the exciton are discussed. The different shapes of the QD, the roughness of the QD wall, and the impurity and defect cases are investigated. In Sec. IV we presented a discussion of the PL spectra and we argued about a possible origin for the modulations on the PL in applied magnetic field. Section V contains the conclusions and final remarks.

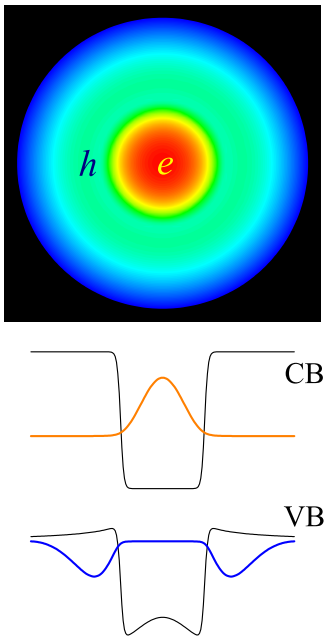

FIG. 1. (Color online) Charged carrier distribution of the type-II quantum dot and the band-edge potentials for the electron and hole within the approximation of separable wave functions, i.e., the Coulomb attraction is included only for the hole.

II. THEORETICAL MODEL

The QD is modeled as a two-dimensional system in a situation favoring the electron to stay inside the dot (assumed to be made of InP) and the hole outside (assumed to be GaAs) as shown in Fig. 1. In order to calculate the exciton energy levels in the presence of a magnetic field B, applied perpendicularly to the dot plane, we have generalized a method based on the solution of the time-dependent Schrödinger equation for two particles within the effective-mass approximation.[13] The Schrödinger equation in this case is given by

$$i\hbar\frac{\partial\psi(\mathbf{r}_e,\mathbf{r}_h,t)}{\partial t}=H\psi(\mathbf{r}_e,\mathbf{r}_h,t), \tag{1}$$

and the exciton Hamiltonian is

$$H=T_e+T_h+V_e(\mathbf{r}_e)+V_h(\mathbf{r}_h)-\frac{e^2}{\epsilon|\mathbf{r}_e-\mathbf{r}_h|}, \tag{2}$$

where $T_e=(\mathbf{P}_e-e\mathbf{A})^2/2m_e$ and $T_h=(\mathbf{P}_h+e\mathbf{A})^2/2m_h$ are the kinetic-energy operators for the electron and the hole, respectively, $\mathbf{A}=(-yB/2,xB/2,0)$ is the vector potential, $V_{e(h)}$ is the electron (hole) confining potential defined as[14] $V_e=130$ meV outside the dot region and 0 inside the dot ($V_h=110$ meV inside the dot and 0 outside the QD), $m_e=0.077m_0$ is the electron effective mass (taken to be isotropic for InP), $m_h=0.5m_0$ is the hole effective mass (taken to be isotropic for GaAs), m_0 is the free-electron mass, and $\epsilon=12.83$ is the average dielectric constant of InP and GaAs. The spin degrees of freedom, as well as the Zeeman splitting (linear in B) associated with them, are not included in the present work, which only addresses the envelope orbital part

of the exciton states. These spin-dependent effects can be important if spin mixing leads to occupation of the dark excitonic states. However, to address properly this effect on the PL signal one should consider the dynamics of the excitation and relaxation of the photoexcited carriers, which is beyond the scope of this paper.

As already mentioned, strain-induced effects are important in determining the electronic distribution around the QD in a three-dimensional system. The inclusion of strain in our two-dimensional model could be done using a modification of the band offset potentials, which unfortunately occurs in an unknown manner in actual samples, since it depends on the particular growth process of the QD. To avoid these uncertainties, and to focus primarily on the effect of the magnetic field on the exciton states, we do not include strain in the present calculation.

The solution of the Schrödinger equation is obtained from the time evolution of the wave functions, which can be accomplished by the formal expression for advancing the wave function by one time-step Δt,

$$\psi(\mathbf{r}_e,\mathbf{r}_h,t+\Delta t) = e^{-iH\Delta t/\hbar}\psi(\mathbf{r}_e,\mathbf{r}_h,t). \quad (3)$$

This operation conserves the normalization of the wave function since the operator is unitary. In general, it is not possible to perform the exponentiation of an operator exactly; then the expression above can be approximated by

$$\psi(\mathbf{r}_e,\mathbf{r}_h,t+\Delta t) \simeq e^{-iV(\mathbf{r}_e,\mathbf{r}_h)\Delta t/2\hbar}e^{-iT_e\Delta t/\hbar} \times e^{-iT_h\Delta t/\hbar}e^{-iV(\mathbf{r}_e,\mathbf{r}_h)\Delta t/2\hbar}\psi(\mathbf{r}_e,\mathbf{r}_h,t). \quad (4)$$

The error introduced in this expression is of order of Δt^3 and it results from the fact that kinetic and potential operators do not commute. The eigenstates of H are obtained by performing the evolution of the wave functions at the imaginary time domain, that is, we substitute t by $-i\tau$. An initial wave function is chosen and propagated using Eq. (4); after few time steps the wave function converges to the ground state of the system. The excited states can also be obtained using the same procedure but imposing orthonormalization between the states. These excited states are important for the present case of type-II QD because the hole is only weakly bound to the electron, demanding the calculation of a large number of close-energy excited states to properly obtain certain observables such as the intensity of the PL signal. It is important to point out that this method does not rely on expansion of basis set of wave functions, which in this specific case, is crucial due to the competition between Coulomb and magnetic field. Here, both contributions are treated on equal footing. It is also not restricted to small fields and there is no free adjustable parameter in this calculation.

The method described above for solving two interacting particles in two dimensions is, however, computationally demanding when including a large number of excited states. After we have done some tests, and in order to speed up the numerical processes, we have approximated the exciton problem by separable wave functions for the electron and for the hole, that is,

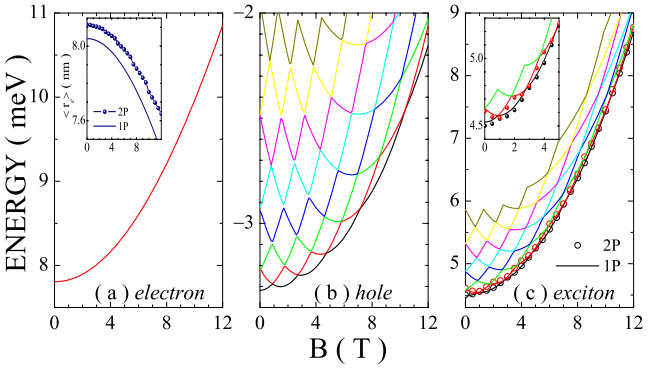

FIG. 2. (Color online) Energies as function of the magnetic field. (a) Electron ground state. The inset shows the average radius $\langle r_e\rangle = \int d\mathbf{r}_h \int d\mathbf{r}_e |\psi(\mathbf{r}_h,\mathbf{r}_e)|^2 r_e$ for the ground-state electron as a function of the magnetic field. (b) Hole ground state and the first few excited states. (c) Exciton states, i.e., the sum of the electron and hole energies. Dots are the result of the exact calculation with two interacting particles for the two lowest-energy states. Lines are the results of the approximative calculation with the separable wave functions. The inset shows an amplified graph for low-field values.

$$\psi(\mathbf{r}_e,\mathbf{r}_h,t) \simeq \psi_e(\mathbf{r}_e,t)\psi_h(\mathbf{r}_h,t). \quad (5)$$

This approximation is still good in this particular problem because the electron is strongly bound inside the QD, therefore it is weakly perturbed by the Coulomb attraction with the hole. For the latter, however, this attraction is crucial to bind the electron-hole pair into an exciton. The approximative solutions are obtained in the following way. We have first calculated the electron states as a function of the magnetic field neglecting the presence of the hole. For the range of energy investigated, only the ground state for the electron suffices. Then the hole states are calculated for the same B-field values, now including the Coulomb attraction with the electron according to

$$V_{eh}(\mathbf{r}_h) = -e^2 \int d\mathbf{r}_e \frac{|\psi_e(\mathbf{r}_e)|^2}{\epsilon|\mathbf{r}_e-\mathbf{r}_h|}. \quad (6)$$

As already said, for the hole, due to the weak confining potential Eq. (6) in type-II QDs, a large number of states have to be calculated since they are very close in energy to each other.

III. RESULTS AND DISCUSSIONS

In addition to the effective masses and the dielectric constant already given above, the results depend also on the physical dimensions of the system and on the intensity of the applied magnetic field. We have investigated circularlike QDs with the dot radius of order of 10–20 nm, similar to the ones studied in actual samples,[15] and varied the field from $B=0$ to 12 T.

In the panels of Fig. 2 we show, for a circular QD of radius 17 nm, the electron energy [Fig. 2(a)] only the ground state is shown, the first-excited state is 20.7 meV above it] and the energy of few hole states [Fig. 2(b)] as function of B. These results were obtained with the procedure described

above using separable wave functions to calculate the exciton. The exciton energy is shown in Fig. 2(c), where it is also presented the results for the calculation done without separating the wave functions, that is, solving the two interacting particles exactly. We observe that the increase of B yields a parabolic energy shift for the electron, as seen in Fig. 2(a), and the electron's angular momentum is equal to zero for the whole field range. Similarly for the hole states, which now exhibit energy-level crossings between states with different orbital angular momenta L_z. In Figs. 2(b) and 2(c), for $B=0$ T, the hole (exciton) ground state has $L_z=0$ and the excited states form a series of twofold-degenerate states with $L_z=\pm m$ (all in units of $\hbar$), with $m=1,2,3,\ldots$ As the field increases, the degenerate states split and then crossings of the energy levels are observed. Notice that the ground state, at each level crossing, changes its angular momentum and the variation on the field needed to produce the change is in accordance with an integer of the magnetic flux picked up by the hole wave function. This is the essence of the X-ABE.

Comparing in Fig. 2(c) the results of the calculations made using the two interaction particles (exact approach) and the separable wave functions (approximative approach), we observe a reasonably good agreement for the lowest-energy states. This is a consequence of the strong confinement of the electron inside the QD, as it can also be seen in the inset of Fig. 2(a) for the small variation of the electron distribution average radius (which varies only 0.4 nm) with increasing B. On the other hand, for the hole in the ground state (not shown), the average radius varies from ~ 29 to ~ 26 nm with B varying from 0 to 12 T. In view of this good agreement between exact and approximative calculations, we use the latter in what follows because it speeds up the numerical calculations, which have to include a large number of excited states.

In Fig. 3 we present three energy spectra as a function of B for a QD of cylindrical shape [radius 17 nm, Fig. 3(a)], for an elliptical QD which keeps the same area of the previous QD [16×18 nm^2, Fig. 3(b)], and for another elliptical QD [14×20.6 nm^2, Fig. 3(c)]. The energy spectrum in Fig. 3(a) is the same shown in Fig. 2(c) but now including up to 50 excited states. Comparing the cylindrical QD in Fig. 3(a) and the elliptical ones in Figs. 3(b) and 3(c), we observe the appearance of level anticrossings for the elliptical dots. This is due to the interaction between the levels which for the elliptical dots results in states with a combination of angular-momentum components. Notice that the elliptical shape still retains some symmetry around the Cartesian axes, therefore the anticrossings occur for levels involving angular-momentum components $L_z\simeq 0,-2,-4$, and so on. The electron keeps its angular momentum $L_z\simeq 0$ for the whole field range. In Fig. 4 we show the hole wave functions for the two states anticrossing at $B\sim 3.3$ T in Fig. 3(b), demonstrating the change in their symmetries ($L_z\sim 0$ and -4 going to -4 and 0).

In Figs. 3(a)–3(c), the number of states calculated (50 in the total) is still not enough to reach the continuum of states for which the hole energy would be positive. (For $B=0$ T, the number of states to reach the continuum is about 60.)[16] Notice also that in Fig. 3(a) there is a set of states with different L_z for the first radial state $n=1$ (low energy states)

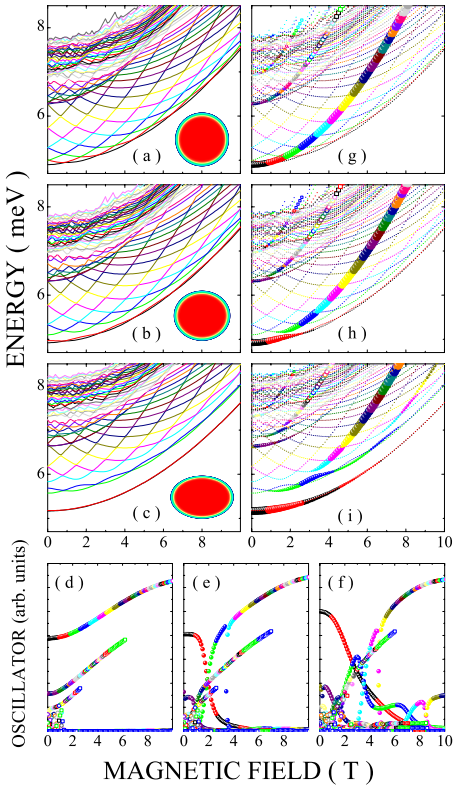

FIG. 3. (Color online) Exciton energy as function of the magnetic field for three different quantum dot geometries, all having the same dot area: [(a), (d), and (g)] the results for a cylindrical dot of radius 17 nm; [(b), (e), and (h)] for an elliptical dot of semiaxes 16×18 nm^2; [(c), (f), and (i)] for an elliptical dot of semiaxes 14×20.6 nm^2. [(a), (b), and (c)] display the magnetoexciton spectra; [(d), (e), and (f)] show the oscillator strength given by Eq. (7); [(g), (h), and (i)] present the spectra with the data points weighted by the oscillator strength.

but there are also other sets of states with different L_z associated with the excited radial states, $n=2,3\ldots$. For the elliptical QDs, we observe that the exciton states at $B=0$ T have the twofold degeneracy lifted and that the ground state and the first excited state do not interact strongly with the other excited states and they appear as side-band states separated from the other states. This is a consequence[17] of the flattening of the QD, which favors the hole state to prefer the Cartesian symmetry than the cylindrical one—the QD appears for these low-energy hole states as a barrier between two large wells, and the hole states behave like the symmetric and the antisymmetric pair of states in a double-well system.

Although the exciton spectra contains many energy levels, only those with a large spatial overlap between the electron and the hole wave functions contribute appreciably to the optical processes. The specific overlap of wave functions, i.e., the optical oscillator strength, is given by

$$f\sim\left|\int d\mathbf{r}\psi(\mathbf{r},\mathbf{r})\right|^2\simeq\left|\int d\mathbf{r}\psi_e(\mathbf{r})\psi_h(\mathbf{r})\right|^2, \qquad (7)$$

where the second expression holds for the approximative calculation with separable wave functions. Figures 3(d)–3(f)

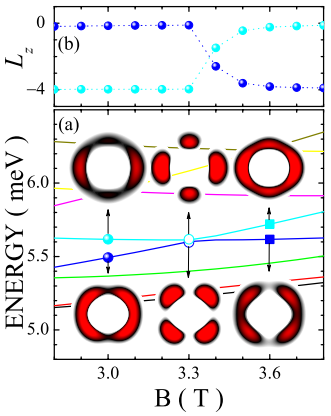

FIG. 4. (Color online) (a) Details of the energy-level anticrossing for the elliptical dot of semiaxes 16×18 nm^2 shown in Fig. 3(b) for field $B\sim3.3$ T. Also shown are the hole distributions around the quantum dot $|\psi_h|^2$ for three values of magnetic field. (b) Angular momentum components $L_z\simeq0$ and −4 of the anticrossing states.

show the overlap f for the cylindrical and ellipsoidal QDs discussed in Fig. 3. Notice that only a few states have appreciable values of f and they have the hole wave function with symmetry similar to the ground-state electron wave function, which is cylindrical or ellipsoidal, therefore mostly like $L_z\simeq0$. We observe that the values of f for the cylindrical QD increases monotonically due to the extra confinement imposed by the magnetic field. For the elliptical QDs, the values of f change significantly for B values in which there is a level anticrossing. The variation of f opens the possibility for observing B-field modulations on optical measurements associated to the X-ABE and we discuss this fact in the next section.

An interesting way of seeing the most important states in the optical processes is to combine the exciton spectra [Figs. 3(a)–3(c)] with their respective overlaps [Figs. 3(d), 3(e), and 3(e)] and create spectra where the data points are weighted by f. This is done for the results in Figs. 3(g)–3(i). These graphs can be seen as the QD absorption spectra, and we can see from them that the most important states for optical processes are not always the lowest-energy states, but those states with angular momentum $L_z\simeq0$. For the cylindrical QD [Fig. 3(g)] we see the $L_z=0$ states associated to different radial states dominating the spectra. For the elliptical QDs [Figs. 3(h) and 3(i)] we observe something similar, but now the $L_z\sim0$ states are interacting with other states (predominantly with those with $L_z\sim-2,-4,\ldots$) due to the cylindrical-symmetry breaking imposed by the QD elliptical shape (see, for example, Fig. 4).

Elongated dots such as the elliptical QDs discussed above may result from the complex growth processes. Another symmetry-breaking effect which is very likely to be found in actual samples is the imperfection of the QD walls. We have modeled these imperfections by creating QDs with rough potential walls, which we have made assuming a random fluctuation on the dot radius according to

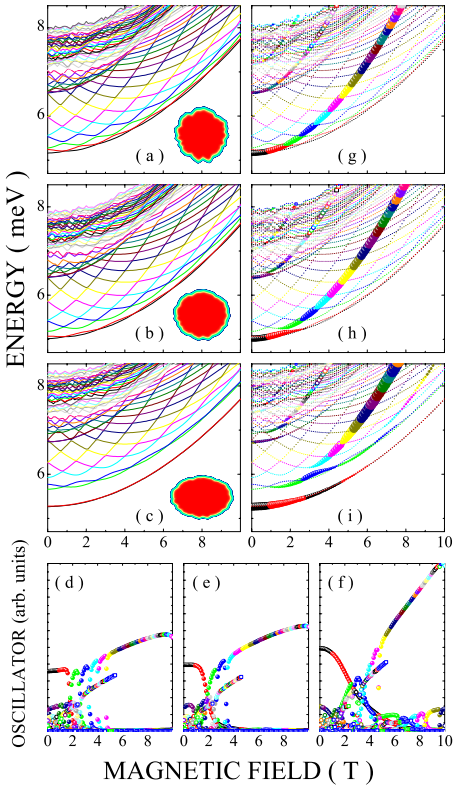

FIG. 5. (Color online) Exciton energy as function of the magnetic field for three different quantum dot geometries, all having the same dot area and with rough walls: [(a), (d), and (g)] the results for a cylindrical dot of radius 17 nm; [(b), (e), and (h)] for an elliptical dot of semiaxes 16×18 nm^2; [(c), (f), and (i)] for an elliptical dot of semiaxes 14×20.6 nm^2. Shown in (a)–(c) are the magnetoexciton spectra; shown in (d)–(f) are the oscillator strength given by Eq. (7); shown in (g)–(i) are the spectra with the data points weighted by the oscillator strength.

$$R(\theta)=R_0+2\sigma_R\sqrt{\frac{L_C}{R_0}}\sum_{n>0}e^{-(nL_C/2R_0)^2}\cos(n\theta+\phi_n),\quad(8)$$

where σ_R is radius dispersion, R_0 is the average radius, ϕ_n is a random phase, and L_C is the correlation length. In Fig. 5 we show the results similar to the ones in Fig. 3, for the same dimensions of QDs, but now including roughness on the dot wall with $\sigma_R=0.5$ nm, $R_0=17$ nm, and $L_C=1.5$ nm. In Fig. 5(a), for a cylindrical QD with rough walls, we observe that the exciton states no longer have pure angular-momentum components. The roughness mixes the L_z components and there are many level anticrossings in the spectra. In Figs. 5(b) and 5(c), the angular momentum mixing already given by the elliptical shape of the dot is enhanced by the wall roughness. The states with larger oscillator strength are still those with $L_z\sim0$, but now these states anticross other states besides those already pointed out in Fig. 3, i.e., $L_z\sim-2$, $-4,\ldots$ for the elliptical case. In Figs. 5(d)–5(f) the squared overlap f exhibiting the effects of the level anticrossings are shown. Figures 5(g)–5(i) give the exciton spectra weighted by f. Again, we observe that the states with $L_z\sim0$ are the most important and that the effect of the anticrossings yields

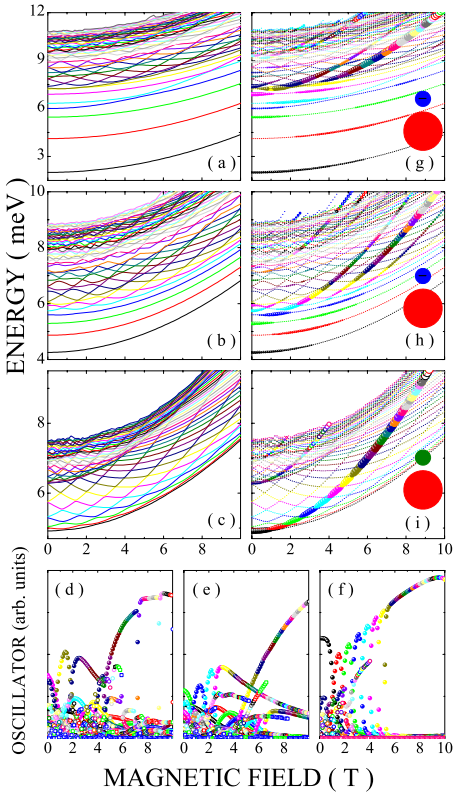

FIG. 6. (Color online) Exciton energy as function of the magnetic field for three different cylindrical quantum dots, all of radius 17 nm: [(a), (d), and (g) the results for negative hydrogenic impurity at (0, 20, 10) nm; [(b), (e), and (h)] impurity at (0, 30, 30) nm; [(c), (f), and (i)] for a positive (Gaussian-type) defect located at (0, 20, 20) nm of intensity 20 meV. (a)–(c) show the magnetoexciton spectra; [(d)–(f)] the oscillator strength given by Eq. (7); and [(g)–(i)] the spectra with the data points weighted by the oscillator strength.

a modulation on the optical intensity of the bright states.

Shallow hydrogenic impurities near the QD also cause the breaking of the cylindrical symmetry.[12] We have investigated a cylindrical QD with one negative-charged impurity close to it, located in the coordinates (x,y,z) with respect to the QD center. The impurity was set somewhat away from the dot otherwise its effects would be too strong and would overcome the electron-hole Coulomb attraction. In Fig. 6 we present the results for a QD of radius 17 nm with impurity at (0,20,10) nm [Fig. 6(a)] and (0,30,30) nm [Fig. 6(b)]. Figures 6(g) and 6(h) give the corresponding spectra weighted by f, which are shown in Figs. 6(d) and 6(e). For weak impurity potential [Figs. 6(b), 6(h), and 6(e)], we see again the mixing of angular-momentum components leading to level anticrossings, but we also see the lower energy states without crossings. This is reinforced in the case of strong impurity potential [Figs. 6(a), 6(e), and 6(h)], for which the lower energy states are even more separated from the excited states. This is a consequence of the strong binding of the holes in these states to the impurity, such that their wave functions do not circulate the QD, therefore inhibiting the X-ABE. For exciton states at higher energy the spectra look more like the previous ones exhibiting X-ABE.

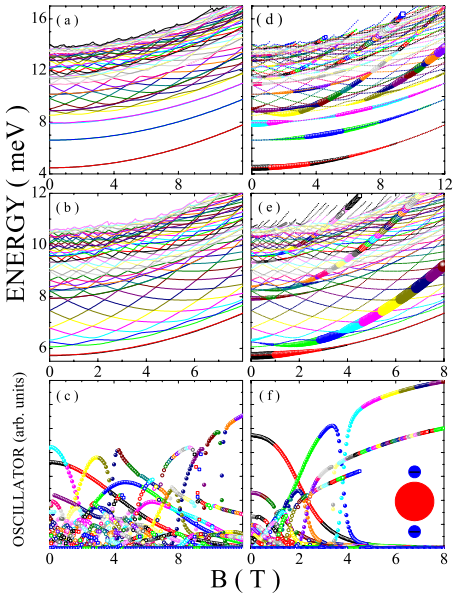

FIG. 7. (Color online) Exciton energy as function of the magnetic field for three different cylindrical quantum dots, all of radius 17 nm: [(a), (c), and (d)] the results for two negative hydrogenic impurities at $(0,\pm 20,10)$ nm; [(b), (d), and (f)] impurities at $(0,\pm 30,30)$nm. (a) and (b) present the magnetoexciton spectra; (c) and (f) the oscillator strength given by Eq. (7); (d) and (e) the spectra with the data points weighted by the oscillator strength.

A similar effect to that of the impurity is the presence of a structural lattice defect near the QD. We simulated the existence of a Gaussian-type defect, with center at (0, 20, 0) nm and radial dispersion 2 nm, having a positive potential, at the center, of $V_0=20$ meV. The results are shown in Figs. 6(c), 6(f), and 6(i). We see an optical spectrum, Fig. 6(i), similar to the cylindrical QD but with sharp anticrossings in almost all angular momentum changes. This is an interesting system because the defect potential is not as strong as the impurity one (such that it would bind the hole), but it is strong enough to break the cylindrical symmetry in a more restrictive way than the elliptical QDs already investigated. This leads to all the level anticrossings.

To verify the rules of symmetry breaking, we have used two impurities located radially symmetric and across the QD as in the work of daSilva *et al.*[12] The results are shown in Fig. 7 for two cases: near impurities located at $(0,\pm 20,10)$ and far impurities located at $(0,\pm 30,30)$. Comparing Fig. 7 to Fig. 6 we observed that the two-impurity system restores some crossings because the system has a higher symmetry than the QD with only one impurity as displayed in Fig. 6. The two-impurity case presents a symmetry that resembles the ellipsoidal QDs, for which there should be less anticrossings.

IV. PHOTOLUMINESCENCE INTENSITY

In trying to get evidence for the X-ABE from optical measurements,[6,8] the experimental studies have looked so far at the energy of the PL peak and at the integrated intensity of the PL signal. The energy shift of the PL peak position is

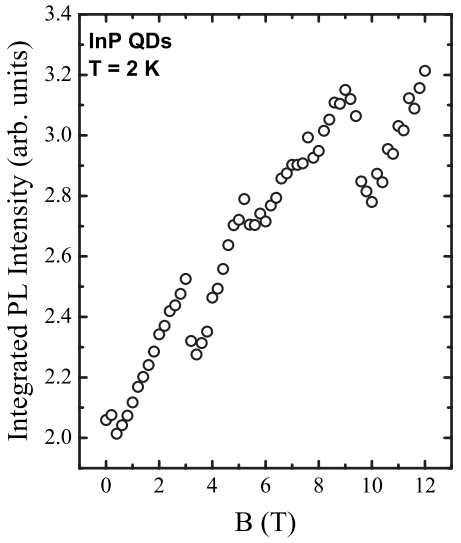

FIG. 8. Low-temperature (2 K) integrated PL intensity as a function of the magnetic field for InP QDs grown on GaAs presenting a type-II band alignment. The integrated intensity presents an overall increase of 60% from 0 to 12 T, but instead of a monotonic increase (expected for a type-I QD), a modulation of the PL, characteristics of Aharonov-Bohm-like behavior, is observed (Ref. 8).

quite small (few millielectronvolt) in comparison with the peak width, the latter resulting from the ensemble of QDs measured. This brings uncertainties into the data analysis. On the other hand, the integrated intensity has shown strong dependence with the applied magnetic field and it may support the optical observation of the X-ABE. Figure 8 presents the measured PL intensity as a function of the magnetic field for InP QDs grown on GaAs that presented the X-ABE.[8] The photoluminescence measurements were performed at 2 K inside a commercial Oxford superconducting magnet, using an Ar ion laser (5145 Å) as the excitation source, focused at a spot of ~ 25 μm in diameter. Sample was probed with 2 W/cm^2, the emission was analyzed by a 0.5 monochromator with a liquid-nitrogen-cooled S1 photomultiplier detector. The magnetic field varied from 0 to 12 T, in 0.2 T steps. For each value of magnetic field a PL spectrum was acquired. All the measurements were performed in a single cool down of the cryostat, and parameters such as light polarization (both incident and emitted), photomultiplier operation temperature, sample temperature, and excitation power were kept fixed. In addition to these experimental parameters, all the optomechanics components were made of Al in order to avoid laser beam deflection with the application of high magnetic fields. These details were important to assure probing the same area of the sample throughout the whole series of PL spectra, leading to a reliable and reproducible sets of data. Sample structure and characterization are given in Refs. 8 and 15. It is seen that instead of a monotonic increase in PL intensity (as one could expect for a type-I band alignment QD) the data exhibit a complicated behavior which is not consistent with the quench in emission intensity predicted for an ideal type-II QD.[1] As already pointed out by the calculations in the previous section, the nonideal nature of the QDs grown by epitaxial techniques will be the key for interpreting the PL intensity data from QDs.

Although from the experimental point of view the PL signal can be easily measured, from the theoretical point of view it is a complicated quantity to be calculated. Besides the proper account of the ensemble of dots being probed, the PL may depend on several excitation and relaxation processes which govern the dynamics of the optically excited electron-hole pairs. Usually the experiments are done by exciting electron-hole pairs high above the exciton absorption line, complicating even more the estimative of the PL signal.

The simplest calculation for the PL intensity can be done considering all excitonic states contributing to the PL, i.e., all states occupied by excitons, and then averaging this population by a thermal (Boltzmann) factor and also by the optical oscillator strength of the transition, Eq. (7), that is,

$$I_{PL} = \frac{\sum_\alpha f_\alpha \exp(-E_\alpha/k_B T)}{\sum_\alpha \exp(-E_\alpha/k_B T)}, \tag{9}$$

where E_α is the exciton energy in the states α, f_α is the overlap integral, and T is the temperature.

The integrated PL intensity I_{PL} calculated in this way for cylindrical QDs does not show B-field modulations, which could be attributed to the X-ABE, because as it is clear from Fig. 3(g) only the $L_z=0$ states contribute and they follow a continuous curve as a function of B. Any fine modulation associated with the interplay between the electron and hole wave functions have to be searched with higher-order derivatives of these curves, making it difficult to be observed experimentally when dealing with ensembles of QDs. On the other hand, for a system with reduced symmetry there are level anticrossings which may favor the observation of the X-ABE in optical measurements. The calculation with Eq. (9), however, tends to hide the X-ABE because the energy differences between the states, as we have shown in the figures above, are very small. This implies that the thermal factor $\exp(-E_\alpha/k_B T)$ is practically constant for anticrossing states. Therefore, the sum over the states in Eq. (9) is approximated by the sum of the oscillator strengths, $\Sigma_\alpha f_\alpha$, which is a constant according to the Thomas-Reich-Kuhn sum rule for the optical oscillator strength. This can be seen from our numerical calculations, for example in Figs. 3(b), 3(e), and 3(h), where close to an anticrossing ($B \simeq 2$ T) the oscillator strengths of the anticrossing states have opposite behavior [one decreases while the other increases, see Fig. 3(e)], but the sum of them is practically constant. This argument is valid no matter which the reason is for breaking the cylindrical symmetry (elliptical dot, roughness of the walls, or impurity). To show that, in Fig. 9 we present the calculation of I_{PL} as defined in Eq. (9) for the cylindrical quantum dot (QD) of Fig. 3(a) [see Fig. 9(a)], for the elliptical QD of Fig. 3(b) [see Fig. 9(b)], for the elliptical and rough-wall QD of Fig. 5(b) [see Fig. 9(c)], for one impurity in Fig. 6(a) [see Fig. 9(d)], for the defect in Fig. 6(c) [see Fig. 9(e)], and for the two impurities in Fig. 7(a) [see Fig. 9(f)]. We do not observe modulations whose origin can be traced to the anticrossings in all these figures, including the one-impurity and defect cases, contrary to the results of Ref. 12 [the approximations used in this work are equivalent to treat the system

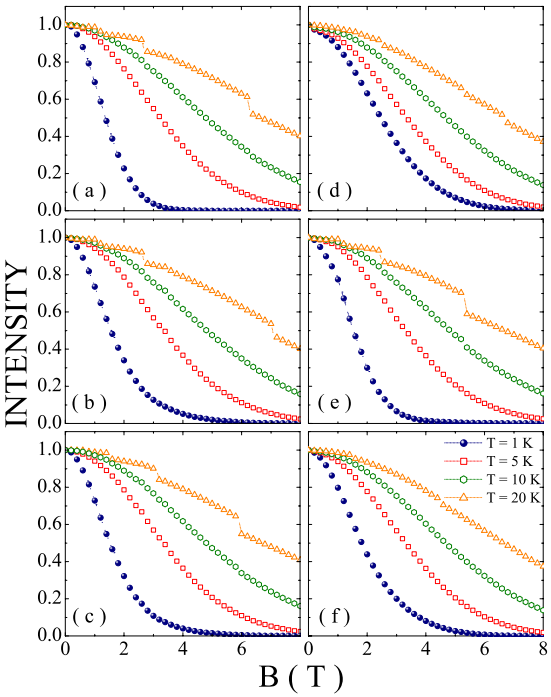

FIG. 9. (Color online) PL integrated intensity as defined in Eq. (9) for different temperatures: (a) For a cylindrical dot with the spectrum showed in Fig. 3(a); (b) For the elliptical QD as in Fig. 3(b); (c) For the elliptical and rough-wall QD as in Fig. 5(b); (d) For one impurity as in Fig. 6(a); (e) For the defect as in Fig. 6(c); (f) For two impurities as in Fig. 7(a). The discontinuities on the graphs of $T=20$ K, at $B\sim 1.2$ T, 2.7 T, and 6 T, are artificial effects resulting from the lack of high-energy excited states in our calculations.

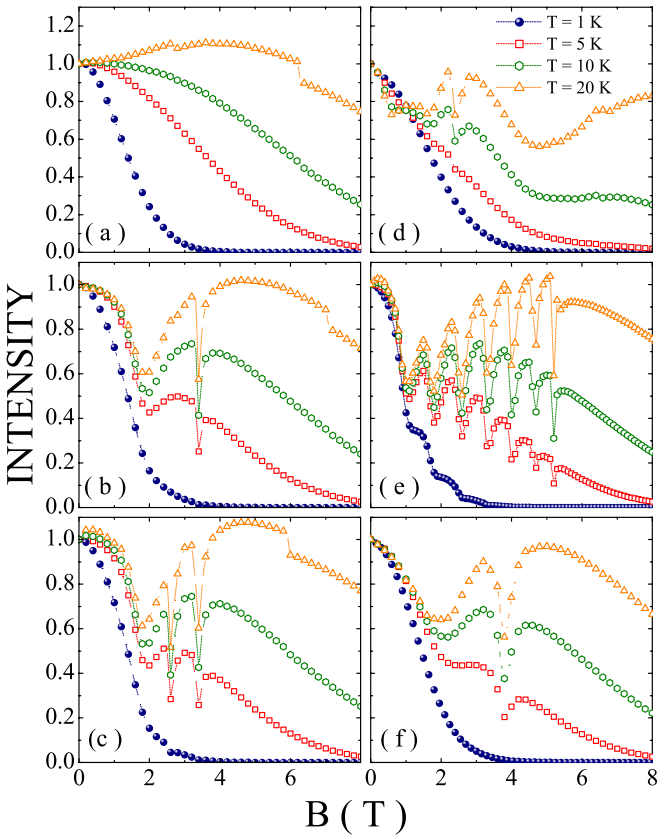

FIG. 10. (Color online) Modified PL integrated intensity [as given by Eq. (10)] for different temperatures: (a) For a cylindrical dot with the spectrum showed in Fig. 3(a); (b) For the elliptical QD as in Fig. 3(b); (c) For the elliptical and rough-wall QD as in Fig. 5(b); (d) For one impurity as in Fig. 6(a); (e) For the defect as in Fig. 6(c); (f) For two impurities as in Fig. 7(a).

as a quantum ring, yielding a larger energy separation between the states, therefore the thermal factor in Eq. (9) can make a difference]. What is observed in Fig. 9 is that the PL intensity decreases with B since the lowest-energy states, which are favored by the Boltzmann factor, loses oscillator strength for increasing B because they are no longer $L_z\sim 0$ like. For increasing temperature, the occupation of highly energetic states become important and the discontinuities on the I_{PL} curves of Fig. 9 result from our limitation in the number of excited states accounted for in Eq. (9).[16]

However, Fig. 8 presents experimental data showing pronounced modulations on the integrated PL intensity as a function of the magnetic field. So the important question to be answered is whether the anticrossings between levels of different angular momenta can be associated with these modulations. If the optical absorption is to be measured, the expected spectra are those shown in this work with the weight of f, for instance Fig. 3(h). With a reasonable precision on the energy scale it would be possible to observe with absorption measurements the anticrossings as a signature of the exciton Aharonov-Bohm effect (X-ABE) for systems with reduced symmetry. In the PL measurements, however, the partial fulfillment of the oscillator-strength sum rule hides the effect. We may question the validity of Eq. (9) arguing about how the exciton population is distributed into the excitonic states. In Eq. (9), besides the thermal factor, all states are assumed equally likely. There are, however, possibilities of restricting the occupation of some states based on the type of relaxation processes the electron-hole pair undergo after optical excitation. For instance, if the excitation is quasiresonant, it would be possible to invoke the conservation of the exciton angular momentum, which is initially $L_z=0$ when optically excited. After relaxation, if there is a partial conservation of these angular momenta, then the sum in Eq. (9) should account for it. As a crude way of obtaining an upper limit to this probability of angular-momentum conservation, we could calculate a modified I_{PL} including the probability of creating the exciton with a certain angular momentum and assuming it to be conserved up to recombination. One would expect an extra f factor, accounting for the selective absorption, in Eq. (9), i.e.,

$$I_{\mathrm{modified}} = \frac{\sum_\alpha f_\alpha^2 \exp(-E_\alpha/k_BT)}{\sum_\alpha \exp(-E_\alpha/k_BT)}. \tag{10}$$

The result, of course, no longer fulfills the sum rule and the modulations on the PL intensity should be observed. In Fig. 10 we reproduce the results shown in Fig. 9, now using the modified PL intensity Eq. (10). We clearly see the modula-

tions on I_{PL} whose origins are the anticrossings in the exciton energy spectra; these structures resemble the experimental curve for a type-II QD (Fig. 8), reinforcing the significance of considering the influence of symmetry-breaking mechanisms when predicting the optical behavior of magnetoexcitons in QDs. However, the experimental data of Fig. 8 show an increase of the PL intensity with the magnetic field, which we could not reproduce neither in Fig. 9 nor in Fig. 10. This indicates that the real circumstance the experiment is performed is much more complex than our model can simulate. On the other hand, the similar measurement in Ref. 6 is better reproduced by our simulation.

V. CONCLUSION

In conclusion, we have investigated magnetoexcitons in type-II QDs in a planar structure. In order to assess the influence of the symmetry reduction on the electronic states as a function of the magnetic field, we varied both the shape (from circular to elliptical) and the environment (rough walls, presence of hydrogenic impurities, and lattice defect nearby) of the QD. We observed that the reduction of the cylindrical symmetry of the dots mixes the exciton orbital angular-momentum components creating level anticrossings when varying the magnetic field. The optically bright excitons were those with angular-momentum components $L_z \simeq 0$, which were not always the ground state when the magnetic field is applied. The ground state loses optical oscillator strength for increasing B field since it changes its angular momentum, no longer being $L_z \simeq 0$. Therefore, the optical observation of the X-ABE, i.e., the change of the angular momentum of the ground-state exciton with B, can be problematic. Nevertheless, it is still possible to have B-field modulations on the exciton optical spectra since the anticrossings of the stronger bright exciton with other states have effects on the optical oscillator strength and on the exciton energy. We discussed, however, that the PL-integrated intensity can hide this modulations because of the partial fulfillment of a sum rule in view of the proximity, in energy, of the exciton states, at least for the type-II QDs we investigated. This does not mean the B-field modulations experimentally observed on the PL integrated signal may not be the result of such anticrossings because as we argued, there can be situations in which the PL can reveal the existence of these anticrossings either by exciton relaxation processes, which restrict the occupation of some states (as discussed in connection with Fig. 10), or for systems in which the exciton states are more separated in energy, such that the thermal factor in Eq. (9) would not allow the sum rule to be fulfilled.

Our work has addressed a simple model of the type-II QD, restricting the charged carriers into a plane and investigating different ways of breaking the cylindrical symmetry of the QD. Nonetheless, its simplicity already reveals the rich phenomenological realm presented by the optical properties of type-II QDs. Our results pointed out that in order to understand the existing experimental data, such as the modulations in PL intensity discussed here, it is most important to model the system as close as possible to the experimentally known imperfections of actual samples since these may determine whether effects such as the X-ABE might be observable or not.

ACKNOWLEDGMENTS

M.H.D. gratefully acknowledges financial support by Dhiminsky ATA. Financial support from CNPq (GMR and ER) is also acknowledged. The magnetic-field measurements were performed at the Group of Optical Properties laboratories, at University of Campinas.

*mhdegani@hotmail.com

[1] A. V. Chaplik, Pis'ma Zh. Eksp. Teor. Fiz. **62**, 885 (1995); [JETP Lett. **62**, 900 (1995)].
[2] D. S. Citrin and A. V. Maslov, Phys. Rev. B **72**, 073302 (2005).
[3] Y. Aharonov and D. Bohm, Phys. Rev. **115**, 485 (1959).
[4] A. O. Govorov, A. V. Kalameitsev, R. Warburton, K. Karrai, and S. E. Ulloa, Physica E (Amsterdam) **13**, 297 (2002).
[5] J. R. Madureira, M. P. F. de Godoy, M. J. S. P. Brasil, and F. Iikawa, Appl. Phys. Lett. **90**, 212105 (2007).
[6] I. L. Kuskovsky, W. MacDonald, A. O. Govorov, L. Muroukh, X. Wei, M. C. Tamargo, M. Tadic, and F. M. Peeters, Phys. Rev. B **76**, 035342 (2007).
[7] Z. Xu and P. M. Petroff, J. Appl. Phys. **69**, 6564 (1991).
[8] E. Ribeiro, A. O. Govorov, W. Carvalho, Jr., and G. Medeiros-Ribeiro, Phys. Rev. Lett. **92**, 126402 (2004).
[9] M. P. F. de Godoy, P. F. Gomes, M. K. K. Nakaema, F. Iikawa, M. J. S. P. Brasil, R. A. Caetano, J. R. Madureira, J. R. R. Bortoleto, M. A. Cotta, E. Ribeiro, G. E. Marques, and A. C. R. Bittencourt, Phys. Rev. B **73**, 033309 (2006).
[10] K. L. Janssens, B. Partoens, and F. M. Peeters, Phys. Rev. B **64**, 155324 (2001); **66**, 075314 (2002); **67**, 235325 (2003).
[11] M. Grochol, F. Grosse, and R. Zimmermann, Phys. Rev. B **74**, 115416 (2006).
[12] L. G. G. V. Dias da Silva, S. E. Ulloa, and A. O. Govorov, Phys. Rev. B **70**, 155318 (2004).
[13] M. H. Degani, Appl. Phys. Lett. **59**, 57 (1991).
[14] B. Wang and S. J. Chua, Appl. Phys. Lett. **78**, 628 (2001).
[15] E. Ribeiro, R. L. Maltez, W. Carvalho, Jr., D. Ugarte, and G. Medeiros-Ribeiro, Appl. Phys. Lett. **81**, 2953 (2002).
[16] We have run all the numerical programs in our home computer (typically Pentium-4, 2.8 GHz, 512 MB of RAM). It took us about a week to obtain a graph for a particular system.
[17] D. Berman, O. Entin-Wohlman, and M. Ya. Azbel, Phys. Rev. B **42**, 9299 (1990).